Experimental Study on Bond Behavior between CFRP Plates and Steel Substrates Using Digital Image Correlation

Hai-Tao Wang[1]; Gang Wu[2]; Yun-Tong Dai[3]; and Xiao-Yuan He[4]

Abstract: The bond between carbon-fiber-reinforced polymer (CFRP) and steel is crucial for strengthening of steel structures using CFRP materials. However, existing studies on this issue are still limited. To better understand the bond behavior of CFRP-to-steel bonded interfaces, this paper reports an experimental study on the behavior of CFRP plate-to-steel bonded joints with a nonlinear adhesive by the single-shear testing method. The three-dimensional digital image correlation (3D-DIC) technique was used to measure the displacements and strains of the specimens. The effects of the bond length and adhesive thickness on the bond behavior are evaluated. The results show that failure occurred within the adhesive layer (i.e., cohesive failure) for all tested specimens. The ultimate load increased with increasing bond length until the effective bond length was reached. The ultimate load also increased as the adhesive thickness was increased from 0.5 to 2.0 mm. The bond-slip relationship exhibited an approximate trapezoidal shape for such bonded joints. The key parameters of the trapezoidal bond-slip relationship were obtained for specimens with different adhesive thicknesses. This study indicates that the 3D-DIC technique is suitable for application in studies of the interfacial behavior between CFRP plate and steel. **DOI: 10.1061/(ASCE)CC.1943-5614.0000701.** © *2016 American Society of Civil Engineers.*

Author keywords: Carbon-fiber-reinforced polymer (CFRP) plate; Bond behavior; Steel; Digital image correlation; Bond-slip relationship.

Introduction

Carbon-fiber-reinforced polymer (CFRP) has been widely used for the strengthening of infrastructure structures. CFRP debonding is the most common failure mode for concrete structures that are strengthened in this manner, and thus, numerous experimental, theoretical, and numerical studies of the bond behavior between CFRP and concrete have been conducted (Taljsten 1994; Chen and Teng 2001; Lu et al. 2005; Ali-Ahmad et al. 2006; Shi et al. 2013). In recent years, the use of CFRP to strengthen steel structures has been attracting increasing attention. Some studies have indicated that CFRP can effectively enhance the flexural, buckling, and fatigue behavior of steel members (Al-Saidy et al. 2004; Harries et al. 2009; Liu et al. 2009; Sallam et al. 2010; Wang et al. 2015). Nonetheless, CFRP debonding may occur in the discontinuous regions (i.e., steel cracks and CFRP terminate locations) and steel yielding zones of CFRP-strengthened steel structures (Deng and Lee 2007; Sallam et al. 2010; Kim and Brunell 2011). Therefore, it is very important to understand the bond behavior between CFRP and steel substrate. However, relevant studies on this issue remain very limited compared with studies of CFRP-to-concrete bonded interfaces.

The behavior of simple bonded joints is of fundamental importance to the understanding of the bond behavior between CFRP and the substrate materials (Teng et al. 2012). The bond-slip relationship, which can be experimentally obtained through the bonded joint tests, is an essential component for modeling the debonding failure process and predicting the structural behavior of CFRP-strengthened members (Teng et al. 2012; Dai et al. 2013). Existing studies have involved studying the behavior of CFRP-to-steel bonded joints under static loading, cyclic loading, impact loading, and fatigue loading in the ambient environment (Bocciarelli et al. 2009; Wu et al. 2012; Kim et al. 2013; Zhao et al. 2013; Al-Mosawe et al. 2015). The effects of harsh environmental conditions (e.g., temperature, sea water, humidity, ultraviolet radiation, and freeze–thaw cycle) on the bond behavior were also investigated (Zhao et al. 2013; Heshmati et al. 2015). These studies have significantly improved the understanding of the bond behavior between CFRP and steel. However, among of the existing studies, only few studies investigated the debonding and bond-slip behavior of CFRP-to-steel bonded interfaces (Xia and Teng 2005; Fawzia et al. 2010; Akbar et al. 2010; Yu et al. 2012).

Xia and Teng (2005) conducted a study on the effects of the type and thickness of the adhesive on the behavior of CFRP-to-steel bonded joints using single-shear pull-off tests. A simplified bilinear bond-slip model was developed based on the test results. The bond behavior between CFRP sheets and steel was studied by Fawzia et al. (2010) using the double-shear test method. The CFRP modulus, bond length, number of CFRP layers, and adhesive type were treated as the variables. A bilinear bond-slip model was simply proposed based on their experimental and numerical results. In the study of Akbar et al. (2010), a new method was developed to derive the bilinear bond-slip curves of CFRP-to-steel bonded interfaces from the global load-slip curves. The study conducted by Wu et al. (2012) showed that the bond-slip relationship between the

[1]Ph.D. Candidate, Key Laboratory of Concrete and Prestressed Concrete Structures of the Ministry of Education, Southeast Univ., Nanjing 210096, China.

[2]Professor, Key Laboratory of Concrete and Prestressed Concrete Structures of the Ministry of Education, Southeast Univ., Nanjing 210096, China (corresponding author). E-mail: g.wu@seu.edu.cn

[3]Ph.D. Candidate, Dept. of Engineering Mechanics, Southeast Univ., Nanjing 210096, China.

[4]Professor, Dept. of Engineering Mechanics, Southeast Univ., Nanjing 210096, China.

Note. This manuscript was submitted on November 13, 2015; approved on February 5, 2016; published online on May 10, 2016. Discussion period open until October 10, 2016; separate discussions must be submitted for individual papers. This paper is part of the ***Journal of Composites for Construction***, © ASCE, ISSN 1090-0268.

ultra-high-modulus CFRP plate and steel exhibited a bilinear shape when the Sikadur-30 adhesive was used. Yu et al. (2012) studied the full-range behavior of CFRP plate-to-steel bonded joints using the single-shear test method. Test results indicated that the bond-slip curve had an approximate bilinear shape for a linear adhesive but an approximate trapezoidal shape for a nonlinear adhesive. This was the first study where the trapezoidal bond-slip relationship was observed through experimental tests although the trapezoidal bond-slip relationship was also presented by Dehghani et al. (2012). However, the trapezoidal bond-slip curves were determined only for specimens with 1-mm-thick adhesive. Based on a review of the existing studies, it can be concluded that studies on the bond-slip behavior are still limited, and there is an obvious difference in the bond-slip behavior between a nonlinear adhesive bonded joint and a linear adhesive bonded joint. In the previous studies, the relevant tests of bonded joints with a nonlinear adhesive are very scarce. Therefore, many studies still need to be conducted to further understand the behavior of CFRP-to-steel bonded joints with a nonlinear adhesive.

An experimental study is reported in this paper to investigate the behavior of CFRP plate-to-steel boned interfaces with a nonlinear adhesive (Araldite-2015, Huntsman Advanced Materials, Basel, Switzerland). The three-dimensional digital image correlation (3D-DIC) technique was applied to measure the displacement and strain data. Two variables, i.e., the bond length and the adhesive thickness, were considered in this study. The main objectives of this paper are to enhance the understanding of the interfacial behavior of CFRP plate-to-steel bonded joints with a nonlinear adhesive, and to confirm the suitability of the 3D-DIC technique for studying such CFRP-to-steel bonded joints.

Experimental Program

Material Properties

The steel plates used in this study were hot-rolled Q235B plates, in accordance with the relevant Chinese standard [GB 50017-2003 (Chinese Standard 2003)]. Their thickness was 20 mm. Their mechanical properties, determined through coupon tests, are listed in Table 1. Unidirectional pultruded CFRP plates (Sika CarboDur S, Sika, Zurich, Switzerland) were used. Their nominal width and thickness were 50 and 1.4 mm, respectively. Their mean elastic modulus and tensile strength were 165 GPa and 3,100 MPa, respectively, according to the technical data sheet provided by the manufacturer. Their basic properties, determined through coupon tests, are listed in Table 1. Araldite-2015, which is a two-component epoxy paste adhesive, was used to bond the CFRP plates to the steel surfaces. The tested stress-strain curve of Araldite-2015 is plotted in Fig. 1. Compared with a typical linear adhesive (i.e., Sikadur-30, Sika, Zurich, Switzerland) (Fig. 1), this adhesive is strongly nonlinear and ductile and has a high toughness. Its mechanical properties, obtained through coupon tests, are listed in Table 1.

Table 1. Tested Material Properties

Material	Tensile strength (MPa)	Young's modulus (GPa)	Yielding stress (MPa)	Elongation %	Poisson's ratio
Q235 steel	414	198	258	29.4	0.3
CFRP plate	2,760	164	—	1.68	0.28
Araldite-2015	15.1	1.75	—	1.74	0.35

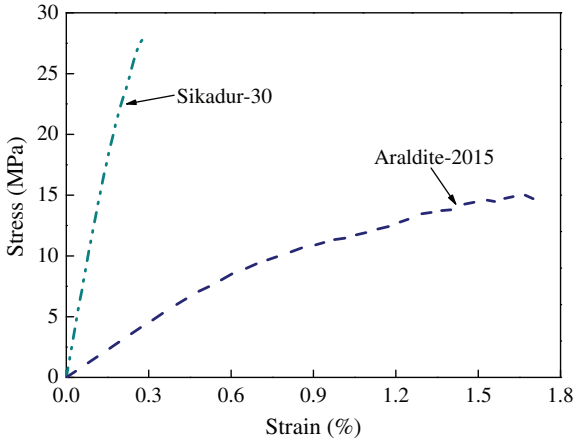

Fig. 1. (Color) Comparison of a typical nonlinear adhesive and linear adhesive

Single-Shear Test Rig

The main test methods used to study the bond behavior of an interface include single-shear test, double-shear test, and beam test. The single-shear test method was recommended by Zhao and Zhang (2007) for the study of the bond behavior between CFRP plate and steel. In this method, there is only one path for debonding, allowing the convenient monitoring of the failure process and derivation of the bond-slip relationship between the CFRP plate and the steel. A special test rig, which was mounted in the test machine, was designed for this study. The bond behavior between CFRP plates and steel substrates can be tested under both static and fatigue loading using this test setup (Wang and Wu 2015). The test rig consisted of a bottom plate, an upper plate, and a steel frame, which were mounted together using four double-screw bolts, as shown in Fig. 2. The specimen was fixed on the test rig using eight bolts, and the steel plate of the specimen was in tight contact with the bottom surface of the upper plate.

Specimen Details

A total of 11 specimens were prepared for this study; the variables were the CFRP bond length and the adhesive thickness, as listed in Table 2. In the specimen identifier, the letter A represents the adhesive, Araldite 2015. The number after the letter represents the

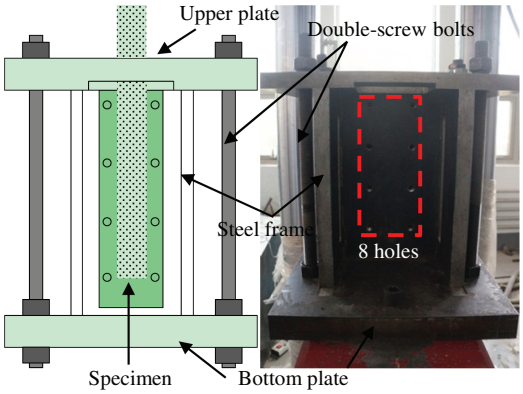

Fig. 2. (Color) Schematic diagram and photograph of the single-shear test rig

Table 2. Specimen Details and Main Test Results

Variable	Specimen identifier	Adhesive thickness (mm)		Bond length (mm)	Ultimate load (kN)	Average bond stress (MPa)	Failure mode[a]
		Designed	Measured				
CFRP length	A70-1.0-1	1.0	0.96	70	52.4	15.0	C
	A90-1.0-1	1.0	1.03	90	78.0	17.3	C
	A110-1.0-1	1.0	0.91	110	73.9	13.4	C
	A130-1.0-1	1.0	0.93	130	90.1	13.9	C
	A150-1.0-1	1.0	1.05	150	112.0	14.9	C
	A350-1.0-1	1.0	0.99	350	108.5	6.2	C
	A350-1.0-2	1.0	1.05	350	109.2	6.2	C
Adhesive thickness	A350-0.5-1	0.5	0.52	350	84.9	4.9	C
	A350-0.5-2	0.5	0.45	350	86.4	4.9	C
	A350-1.0-1	1.0	0.99	350	108.5	6.2	C
	A350-1.0-2	1.0	1.05	350	109.2	6.2	C
	A350-2.0-1	2.0	1.90	350	126.2	7.2	C
	A350-2.0-2	2.0	1.94	350	123.8	7.1	C

[a]C represents cohesive failure.

bond length. The second number represents the design thickness of the adhesive layer. The final number is used to differentiate two nominally identical specimens. For consistency with previous studies by the authors of this paper (Wang et al. 2015), Araldite-2015 was chosen as the adhesive for bonding the CFRP plates. First, the effect of the bond length was investigated by varying the bond length from 70 to 350 mm, and the adhesive thickness for this series of specimens was kept at 1.0 mm. Then, specimens with different adhesive thicknesses were tested to study the full-range behavior and the bond-slip relationship. In these specimens, the bond length was 350 mm, which was much longer than the effective bond length, and the design thickness of the adhesive layer was varied from 0.5 to 2.0 mm. This range of adhesive thickness essentially covers the realistic thicknesses of the adhesive in practical engineering (Xia and Teng 2005).

A schematic diagram of the specimen is shown in Fig. 3. The steel plate had a length of 380 mm, a width of 138 mm, and a thickness of 20 mm. Eight holes of 17 mm in diameter were machined in the steel plate, and these holes were used to fix the specimen to the test rig. The width of the CFRP was 50 mm, its thickness was 1.4 mm, and its total length (L_f) was 420–700 mm, depending on the CFRP bond length. To prevent the CFRP plate from being directly gripped by the grip head and prematurely slipping in the grip zones, anchorage plates were designed for each specimen, as shown in Fig. 3. Each anchorage plate was 250 mm long, 104 mm wide, and 8 mm thick. Several grooves were machined on the inner surface of each anchorage plate to enhance the bond between the anchorage plate and the CFRP plate. Ten holes were drilled in each anchorage plate to admit bolts, which exerted the necessary pressure to anchor the CFRP plate. Six bolts were removed after the adhesive solidified, leaving the specimen gripped only in the plane regions.

Specimen Preparation

The surface treatment of the steel exerts a significant effect on the bond behavior of the CFRP-to-steel interfaces, such as the failure mode and the ultimate load (Hollaway and Cadei 2002; Fernando et al. 2013). Sandblasting has proven to be an effective method for treating the steel surface to avoid failure at the steel–adhesive interface (Fernando et al. 2013). In this study, the surface of each steel plate was first sandblasted to remove rust and contaminants, creating a rough, clean, and chemically active surface. The surface of each CFRP plate was abraded using very fine sandpaper (grit P240) to increase its surface roughness. Before bonding a CFRP plate, the surfaces of both the steel and CFRP plates were cleaned with acetone. The CFRP plate was bonded to the steel surface within 24 h after sandblasting. Precisely machined spacers were used to control the adhesive thickness. The thickness of each spacer was the sum of the CFRP thickness and the design thickness of the adhesive layer. L-shaped steel baffles were also machined in order to avoid CFRP plates from skewing during bonding. The schematic of the bonding procedure is shown in Fig. 4. Table 2 lists the measured and designed thickness of the adhesive layers. The results demonstrate that the adopted method was suitable for controlling the adhesive thickness. All of the specimens were cured at room temperature for at least 2 weeks before testing.

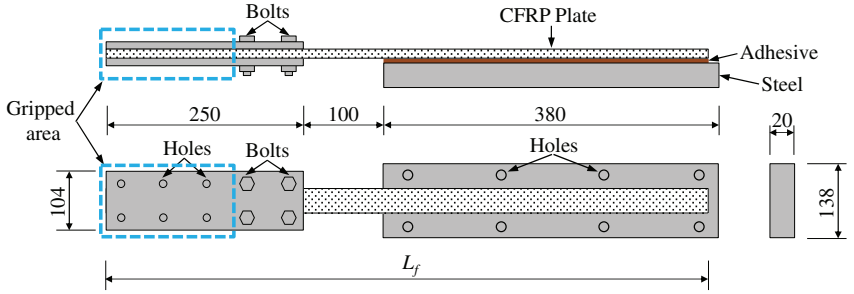

Fig. 3. (Color) Specimen geometry (in mm)

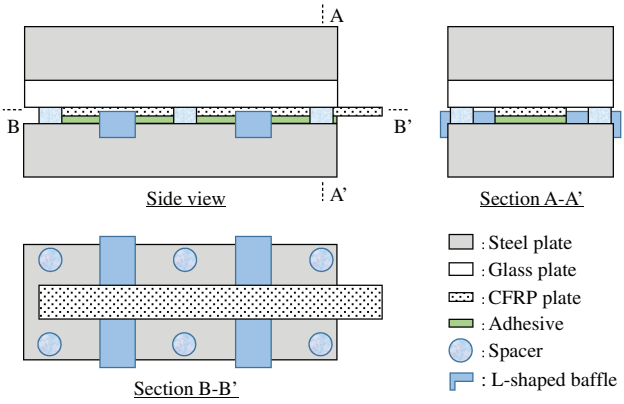

Fig. 4. (Color) Schematic diagram of CFRP bonding procedure (not to scale)

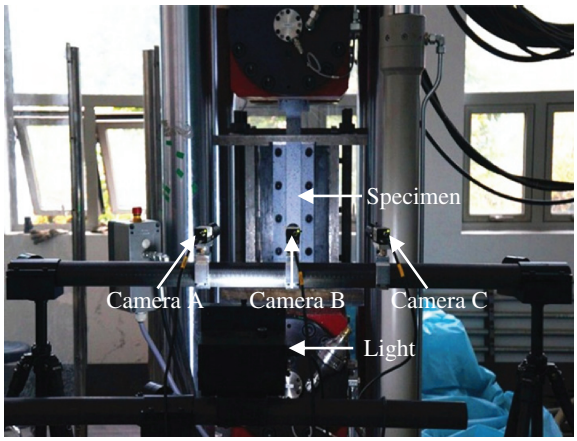

Fig. 5. (Color) Test setup and 3D-DIC system

Loading Procedure and Instruments

The tests were conducted on a servohydraulic testing system (walter+bai ag Testing Machines, Switzerland) with a capacity of 1,000 kN, as shown in Fig. 5. The specimens were loaded under tension until failure occurred by the displacement control at a rate of 0.003 mm/s. The 3D-DIC technique was used to measure the displacements and strains of the specimens. Unlike strain gauges, the DIC method can capture both the continuous displacement and strain fields. This method has previously been used for tests of FRP-to-concrete bonded joints and FRP-to-masonry bonded joints (Carloni et al. 2012; Shi et al. 2013; Wu and Jiang 2013; Ghiassi et al. 2013; Kalfat and Al-Mahaidi 2014). Prior to mounting each specimen in the test machine, white and black matte paint were sprayed onto the test surface of the specimen to produce a random speckle pattern. Before testing, the calibration procedure was performed using calibration boards to determine the geometric relationship between point position on the specimen surface in the 3D space and its corresponding point position on the two-dimensional (2D) images. The DIC images captured by Cameras A and C (Fig. 5) were used to calculate the data during the postprocessing. The displacement and strain data were calculated based on the undeformed and deformed images using *PMLAB 3D-DIC* software. The DIC images were automatically recorded once per second during testing.

Test Results and Discussions

Failure Mode

Various failure modes may occur in CFRP-to-steel bonded joints, such as cohesive failure, CFRP-adhesive interface failure, adhesive-steel interface failure, CFRP delamination, and CFRP rupture (Zhao and Zhang 2007). Teng et al. (2012) recommended that failure should be made most likely to occur in the adhesive layer (i.e., cohesive failure) through the application of a suitable surface treatment in combination with an appropriate adhesive. In this paper, the failure modes observed for all specimens are listed in Table 2, and typical photographs of the specimens after the tests are shown in Fig. 6. It was found that all specimens failed predominantly in the cohesive failure within the adhesive layer, not only demonstrating that the strength of the adhesive was fully utilized but also indicating an appropriate surface treatment and adhesive selection. From the perspective of the failure mode, Araldite-2015 is very suitable for the strengthening of steel structures using CFRP plates. CFRP delamination could also be observed in certain regions of the specimens, which may be caused by deviations in the fabrication of the specimens, nonuniform CFRP quality, or peeling stress near the free end of the CFRP plate. For specimens with 350-mm-long CFRP, the debonding failure progressed gradually from the loaded end toward the free end of the CFRP plate, and the failure process was very ductile. For specimens with a shorter bond length, failure occurred abruptly after the ultimate load was reached without obvious debonding propagation.

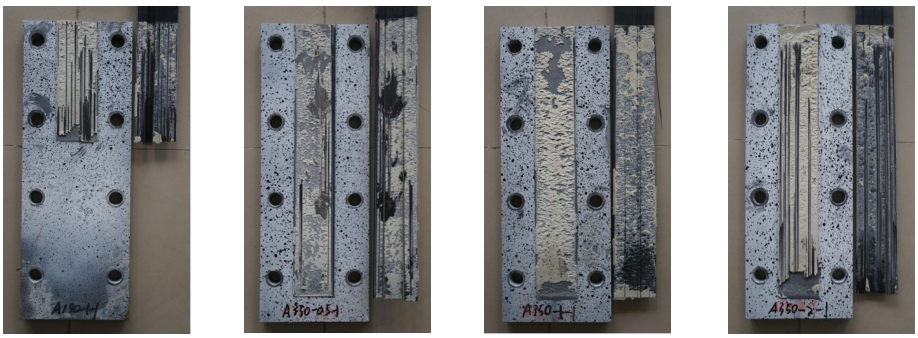

A150-1.0-1 A350-0.5-1 A350-1.0-1 A350-2.0-1

Fig. 6. (Color) Typical failure mode of the specimens

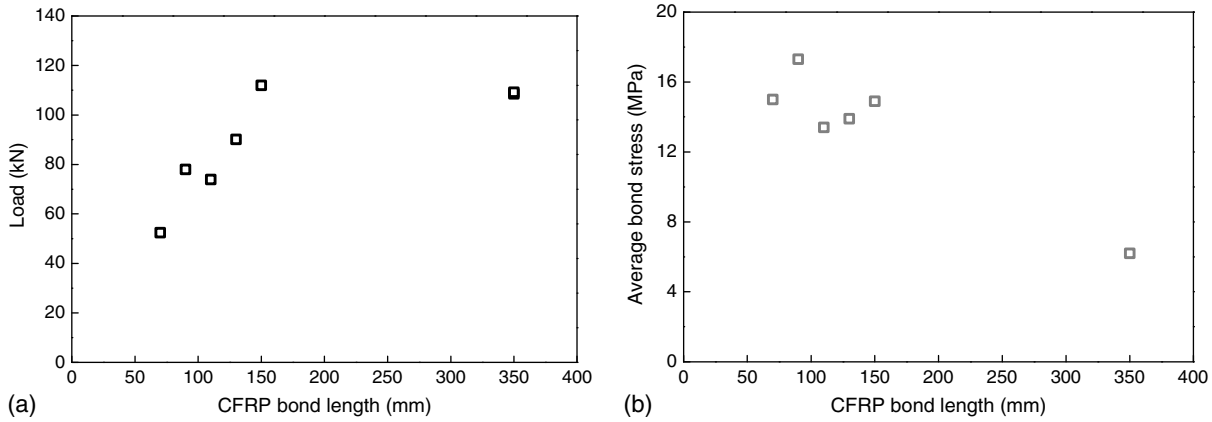

Fig. 7. Effect of the bond length on the ultimate load and average bond stress: (a) ultimate load; (b) average bond stress

Ultimate Load and Average Bond Stress

The ultimate load and average bond stress for each specimen are listed in Table 2. The average bond stress is the ratio between the ultimate load and the bond area. Fig. 7 shows the effect of the bond length on the ultimate load and average bond stress. It can be seen that the ultimate load increased with increasing bond length until a certain bond length value was reached, after which the ultimate load remained approximately constant. The bond length beyond which the ultimate load becomes constant is defined as the effective bond length (Chen and Teng 2001). This indicates that the effective bond length also existed for such CFRP-to-steel bonded joints. Fig. 7(b) shows that the average bond stress exhibited a gradual downtrend with increasing bond length, implying the interfacial-shear stress had a significantly nonuniform distribution along the bond length.

Regarding the effect of the adhesive thickness, it is evident from Fig. 8 that both the ultimate load and the average bond stress gradually increased as the adhesive thickness increased from 0.5 to 2.0 mm. The adhesive thickness may influence the failure modes of CFRP-to-steel bonded joints. Existing studies found that the failure mode could change from cohesive failure to CFRP delamination when the adhesive thickness exceeded 2 mm (Xia and Teng 2005; Yu et al. 2012). The ultimate load would not exhibit this uptrend if the failure mode were to change with an increase in the adhesive thickness. Therefore, an upper limit of 2 mm is recommended for the adhesive thickness.

Displacement and Relative Slip

One of the advantages of 3D-DIC is that the displacement field can be obtained directly, thereby enabling a convenient analysis of the displacement and relative slip distribution. Fig. 9(a) presents the typical displacement distribution on the steel and CFRP surfaces in the width direction for specimen A350-1.0-1. It is evident that the displacement remained approximately constant on both the steel and CFRP surfaces. Because of the impossibility of measuring the displacement of the steel surface covered by the CFRP plate, the relative slip can be considered as the difference between the CFRP and steel displacements [Fig. 9(a)], under the assumption that the displacements of the steel surface remain unchanged along the width direction. Therefore, the continuous relative slip distribution can be obtained using the 3D-DIC method. For the subsequent analysis, the CFRP displacement was obtained as the average value across the 10-mm width of the CFRP in the central region, whereas the steel displacement was taken as the average of the two 5-mm-wide regions on both sides. Fig. 9(b) plots the typical displacement distribution across the steel and CFRP surfaces in the length direction for Specimen A350-1.0-1. The results indicate that the CFRP displacement gradually decreased with increasing distance from the loaded end, whereas the steel displacement remained approximately constant along the length direction. This observation demonstrates that the steel displacement consisted almost entirely of rigid-body displacement induced by the deformation of the steel rods and upper plate, and that the steel substrate suffered relatively

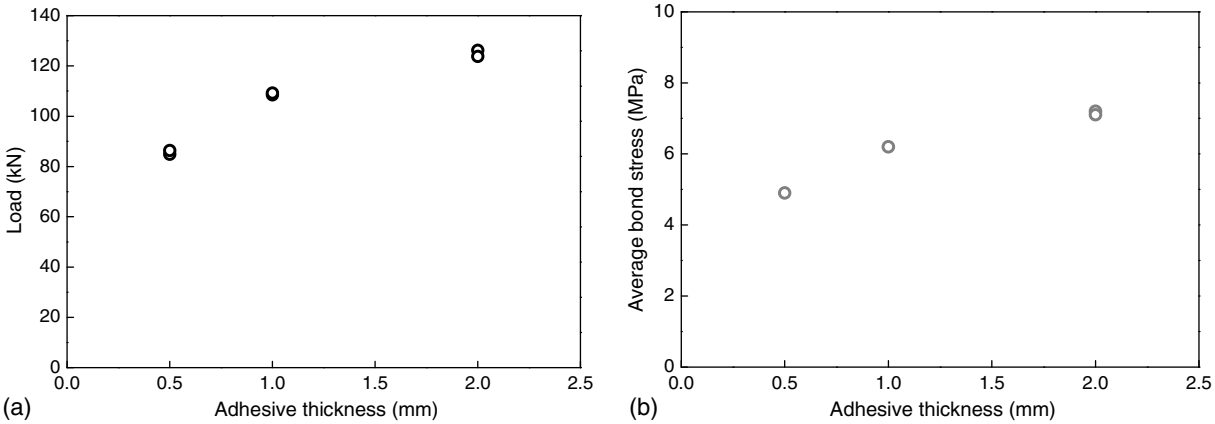

Fig. 8. Effect of the adhesive thickness on the ultimate load and average bond stress: (a) ultimate load; (b) average bond stress

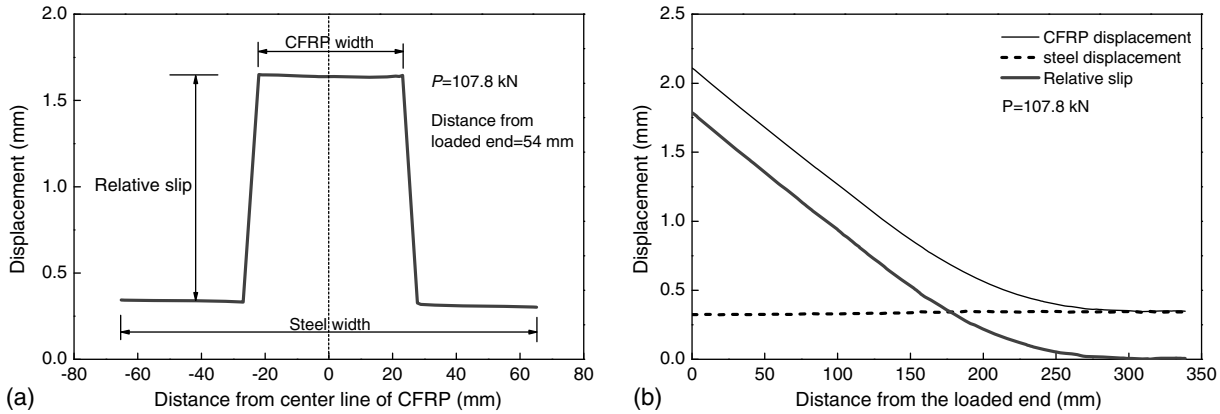

Fig. 9. Typical displacement and relative slip distributions: (a) along the width direction; (b) along the length direction

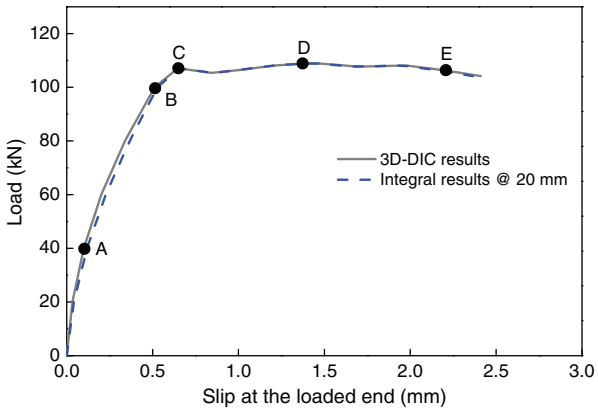

Fig. 10. (Color) Relationship between applied load and loaded-end slip

little deformation during loading. The relative slip between the CFRP plate and steel decreased with increasing distance from the loaded end.

Fig. 10 plots the curve of the applied load versus the loaded-end slip for Specimen A350-1.0-1. It is apparent that the load increased with an increase in the relative slip. The load-slip curve became nonlinear at a very early stage because of the high nonlinearity of the adhesive of Araldite-2015. Debonding first occurred at the loaded end while approaching the Point C marked in Fig. 10, and then the load-slip curve exhibited a broad plateau with increasing relative slip, indicating the gradual debonding process of the interface.

In previous studies, the relative slip was usually obtained by integrating the scattered strain values recorded using strain gauges as follows (Yu et al. 2012):

$$\delta(x_{i+1/2}) = \frac{(\varepsilon_i + \varepsilon_{i+1})}{4}(x_{i+1} - x_i) + \sum_{i}^{n} \frac{(\varepsilon_{i+1} + \varepsilon_{i+2})}{2}(x_{i+2} - x_{i+1}) \quad (1)$$

where ε_i = ith strain value away from the loaded end; x_i = distance from the loaded end at which the ith strain value was recorded; n = the number of strain values used to calculate the relative slip; and $\delta(x_{i+1/2})$ = relative slip at the midpoint between the locations associated with the ith and the ith $+1$ strain value. A comparison of the load-slip curves obtained using the 3D-DIC method and the integral method based on adjacent strain values recorded at 20-mm intervals is also presented in Fig. 10. The results show that the results obtained using two methods are generally similar. The slips calculated using the integral method are slightly larger than the 3D-DIC results in the pre-debonding stage and similar to each other in the debonding stage. This is mainly because the integral method cannot account for the effect of the steel displacement.

CFRP Strain Distribution

The typical strain contours at various stages on the load-slip curve, as marked in Fig. 10, are shown in Fig. 11. Figs. 11(a–c) shows that

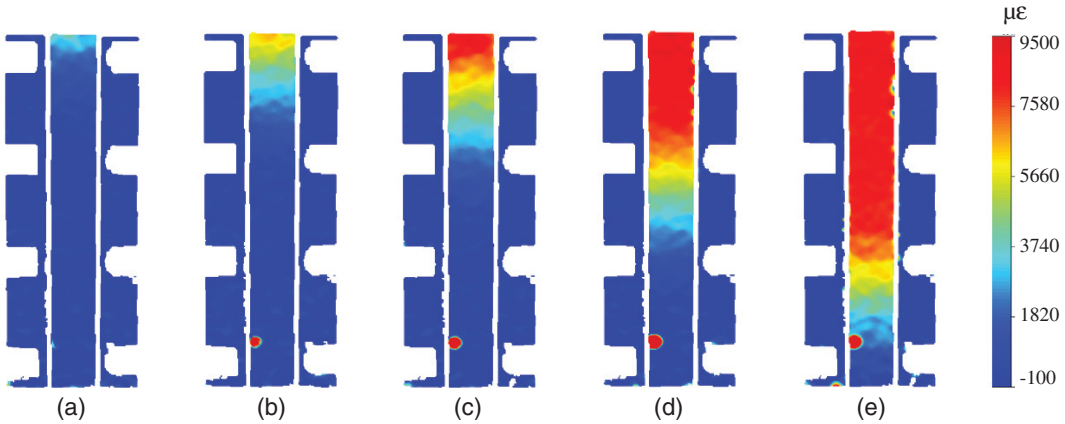

Fig. 11. (Color) Typical CFRP strain contours in various stages of loading: (a) Point A; (b) Point B; (c) Point C; (d) Point D; (e) Point E

a high local strain gradient was observed upon approaching the loaded end and that the local region of this high-strain gradient increased in length with an increase in the applied load. After debonding occurred at the loaded end, as shown in Figs. 11(d and e), the region of the high strain gradient gradually moved down along the CFRP length as the loaded-end slip increased. In this stage, the peak strain remained approximately unchanged and the distribution range of the peak strain gradually increased, confirming the occurrence of progressive debonding propagation as the loaded-end slip increased. It can also be observed from Fig. 11 that the strains on the steel surface were very small compared with the CFRP strains, further demonstrating that the displacements of the steel surface were essentially rigid-body displacements.

Fig. 12 plots the axial strain distribution along the CFRP plate for three specimens with different adhesive thicknesses. This figure reveals similar strain distributions for different specimens. Prior to debonding, CFRP strains developed only within a local region around the loaded end and gradually decreased as increasing

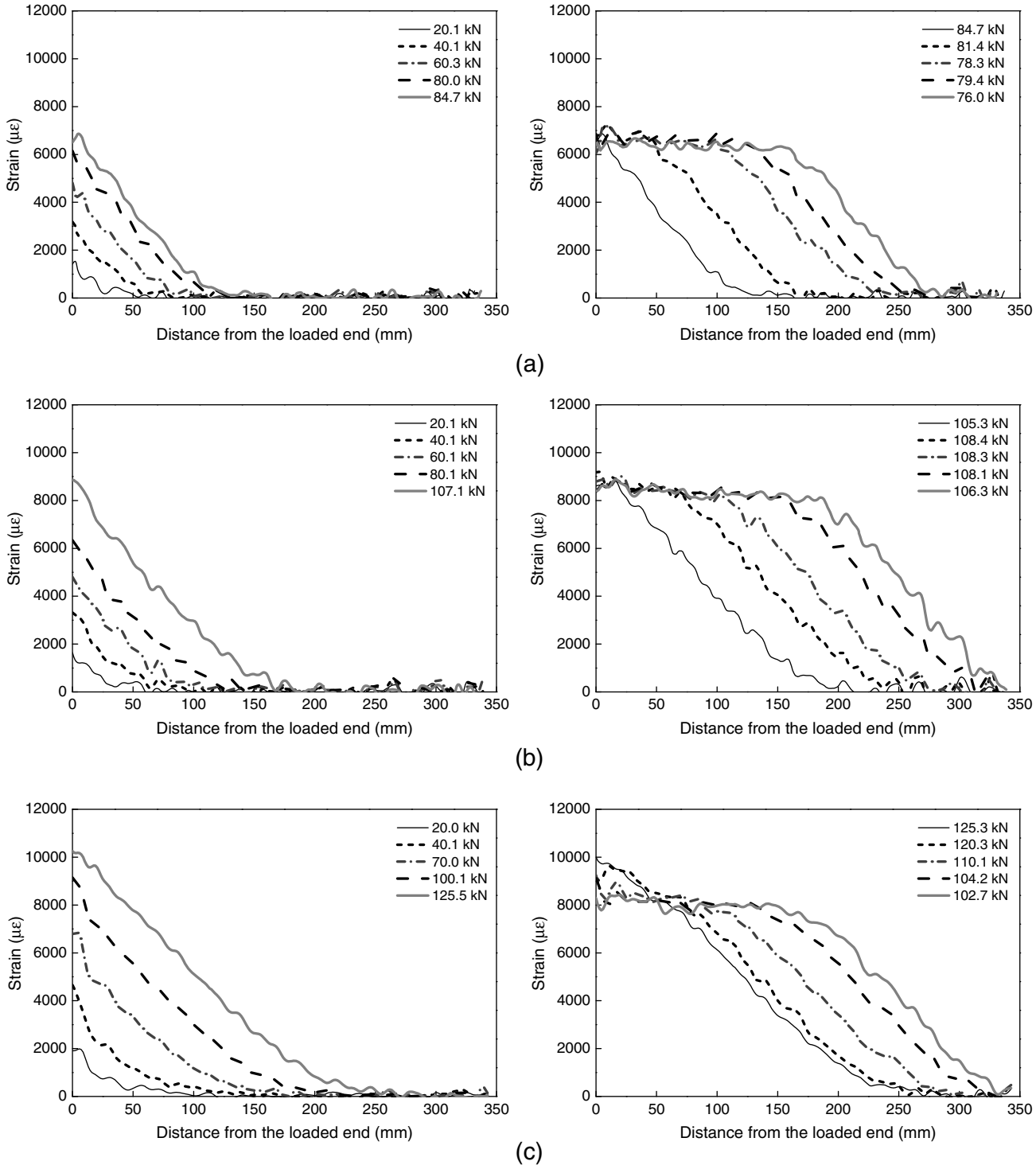

Fig. 12. Typical CFRP axial strain distributions: (a) A350-0.5-1; (b) A350-1.0-1; (c) A350-2.0-1

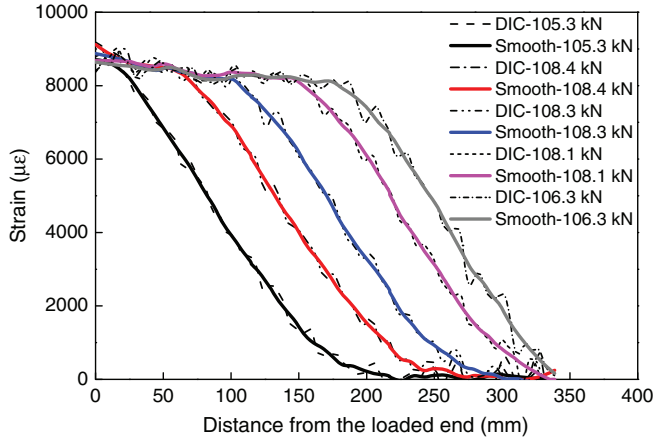

Fig. 13. (Color) Comparison of original and smoothed DIC strains

distance from the loaded end. As the applied load increased, the strains at the loaded end gradually increased, as did the length of the strained region. After debonding occurred at the loaded end, the CFRP strain distribution reached a plateau, and the strains remained approximately constant within this region. This plateau indicated the debonding length of the CFRP plate. The strain distributions beyond the debonding region were similar and propagated gradually toward the free end. Fig. 12 shows that the peak strain increased as the adhesive thickness increased, as did the length of the strained region, which resulted in the larger ultimate loads and longer effective bond lengths for specimens with thicker adhesive.

Interfacial-Shear Stress Distribution

The interfacial stress distribution can reflect the process of stress development and transfer between the CFRP plate and the steel, which can be approximately calculated using Eq. (2)

$$\tau(x_{i+1/2}) = E_f t_f \frac{(\varepsilon_i - \varepsilon_{i+1})}{(x_{i+1} - x_i)} \tag{2}$$

where E_f and t_f = elastic modulus and thickness, respectively, of the CFRP plate; and $\tau(x_{i+1/2})$ = shear stress at the midpoint between the locations associated with the ith and the ith + 1 strain value. As shown in Fig. 12, the strain data obtained from the DIC method exhibited some fluctuations, which would lead to more severe fluctuations of the shear stress if the original strains obtained from the DIC method were directly differentiated. A smoothing method was applied by Shi (2014) to reduce the strain fluctuations of the FRP-to-concrete bonded interfaces, and the results indicated that this method was suitable for processing DIC data. A comparison of the strain distributions before and after the smoothing processing is presented in Fig. 13. It can be observed that the strain fluctuations can be lessened by smoothing and that the smoothed strains can also reflect the strain distributions well. Therefore, the smoothed strains were used to calculate the interfacial-shear stress in the following analysis.

Fig. 14(a) shows the typical interfacial-shear stress distributions along the CFRP plate in different stages of loading for specimen A350-1.0-1. The shear stress distributions for the other specimens were similar. It can be observed that the maximum shear stress was located at the loaded end in the early stage of loading and that the shear stress gradually decreased toward the free end. After the shear stress at the loaded end reached its peak value, a stress plateau gradually developed with an increase in the applied load. With the onset of the softening stage at the loaded end, the shear stress at the loaded end began to gradually decrease. Debonding occurred when the shear stress at the loaded end was reduced to zero. Thereafter, the overall shape of the interfacial shear stress distribution remained similar except that it shifted gradually from the loaded end to the free end of the CFRP plate with the propagation of the debonding. From a comparison with existing studies using a linear adhesive (Xia and Teng 2005; Yu et al. 2012; Wu et al. 2012), it can be found that a linear adhesive exhibited a rather different shear stress distribution compared with a nonlinear adhesive, as shown in Fig. 14(b). In a specimen prepared using a linear adhesive, the shear stress distribution did not contain a stress plateau, and the length of the region in which stress developed was much shorter than in the case of a nonlinear adhesive, resulting in a much lower ultimate load for the linear adhesive.

Bond-Slip Relationship

The bond-slip model describes the relationship between the local interfacial shear stress and the relative slip, which is important for analyzing the behavior of CFRP-strengthened steel structures using analytical and numerical methods (Teng et al. 2012).

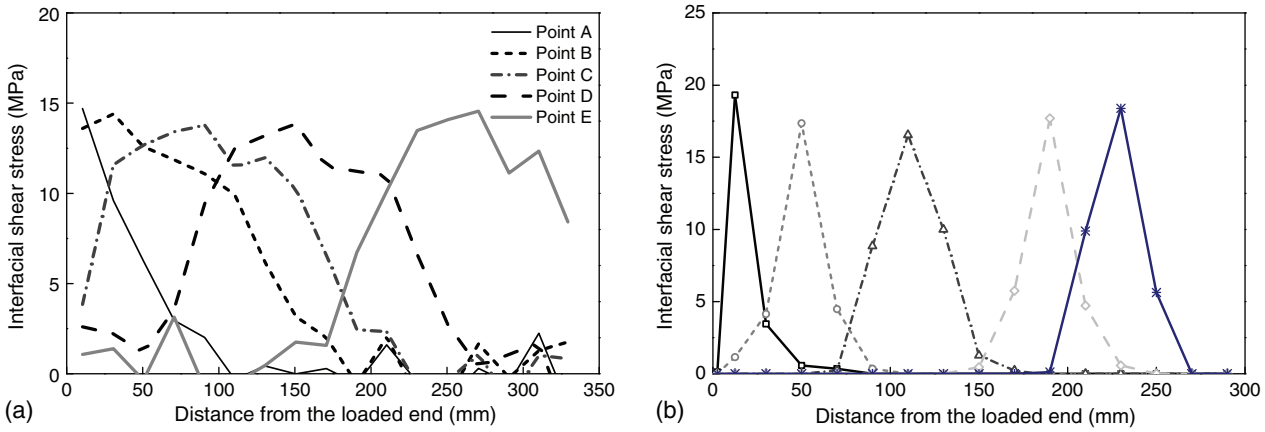

Fig. 14. (Color) Typical interfacial-shear stress distributions: (a) specimen with a nonlinear adhesive; (b) specimen with a linear adhesive (Yu et al. 2012)

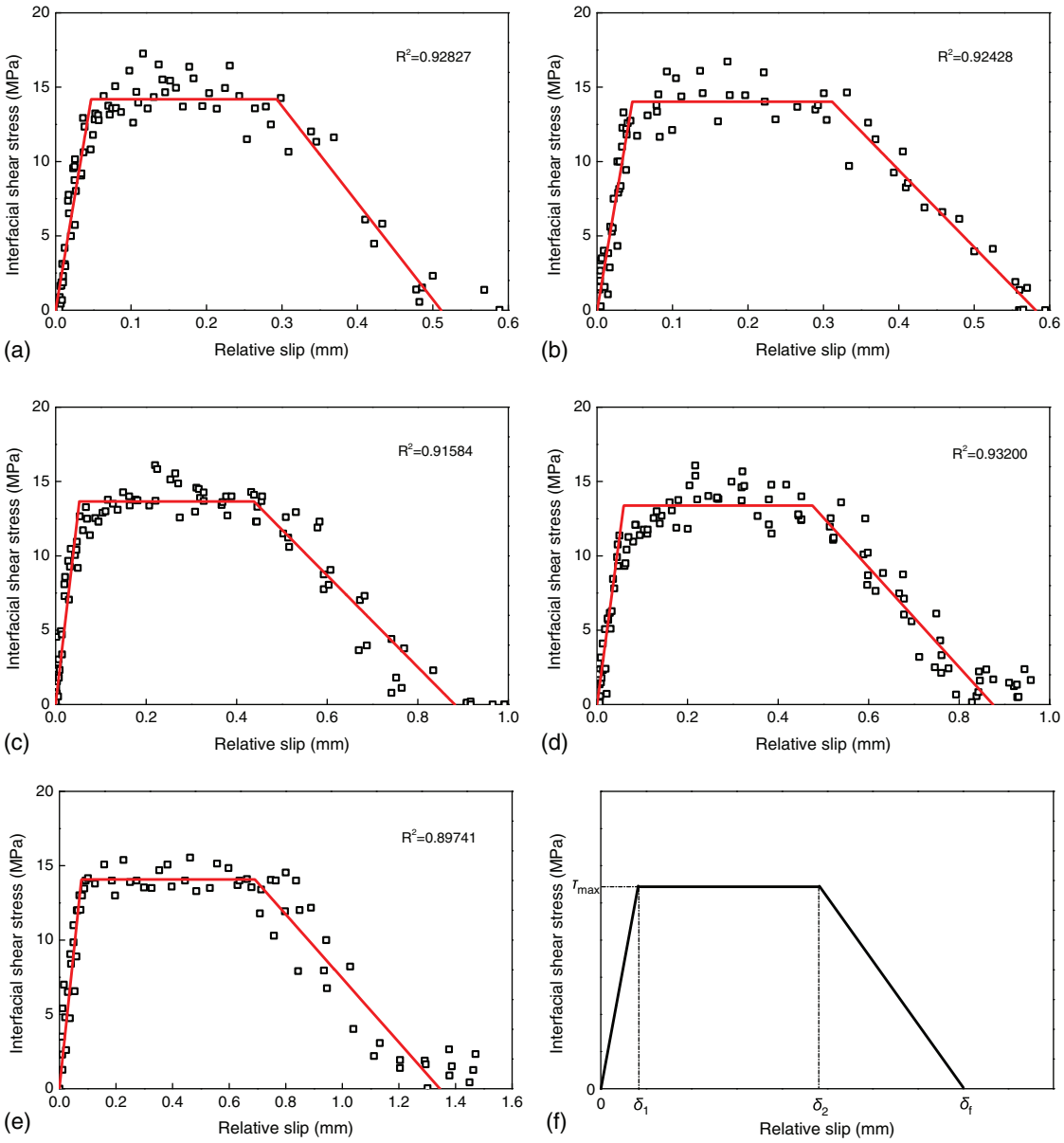

Fig. 15. (Color) Bond-slip relationships of specimens with 350-mm CFRP plates: (a) A350-0.5-1; (b) A350-0.5-2; (c) A350-1.0-1; (d) A350-1.0-2; (e) A350-2.0-1; (f) simplified bond-slip curve

The full bond-slip curve can be experimentally obtained from a specimen with a bond length that is longer than the effective bond length. Fig. 15 shows the experimental bond-slip relationships for the specimens with 350-mm CFRP plates. The 3D-DIC images for Specimen A350-2.0-2 were not recorded completely because the operation of the DIC system failed; thus its bond-slip curve could not be obtained. It can be seen from Figs. 15(a–e) that the bond-slip relationship showed a clear trend for all specimens, which can be essentially divided into three distinctive parts: (1) the ascending branch, in which the shear stress increased with increasing relative slip; (2) the approximate plateau branch, in which the shear stress varied little as the relative slip increased; and (3) the descending branch, in which the shear stress gradually decreased and eventually approached zero with increasing relative slip.

The bond-slip relationship can be simplified to a trapezoidal shape for easy application, as shown in Fig. 15(f). The trapezoidal bond-slip curve can be expressed as follows:

$$\tau = \begin{cases} \tau_{\max} \cdot \frac{\delta}{\delta_1} & \delta \le \delta_1 \\ \tau_{\max} & \delta_1 < \delta \le \delta_2 \\ \tau_{\max} \cdot \frac{\delta_f - \delta}{\delta_f - \delta_2} & \delta_2 < \delta \le \delta_f \\ 0 & \delta > \delta_f \end{cases} \tag{3}$$

where $\tau_{\max}$ = peak interfacial shear stress; δ_1 = value of the relative slip where the ascending branch ends and the plateau branch begins; δ_2 = value of the relative slip where the plateau branch ends and the descending branch begins; and δ_f = peak relative slip where the interfacial shear stress decreases to zero. Four parameters can be used to characterize the bond-slip relationship, i.e., the peak interfacial shear stress $\tau_{\max}$; and the relative slips δ_1, δ_2, and δ_f. Based on the Eq. (3), these parameters can be determined through a least-squares fitting analysis of the experimental bond-slip relationship. The fitted bond-slip curves are also plotted in Fig. 15. The best-fit values of the four parameters for the various specimens are listed in

Table 3. Main Parameters of the Bond-Slip Relationship and Predicted Results

Specimen	$P_{u,\exp}$ (kN)	G_f (N/mm)	$\sigma_{\max}$ (MPa)	δ_1 (mm)	δ_2 (mm)	δ_f (mm)	L_{eff} (mm)	$P_{u,\text{pre}}$ (kN)	$P_{u,\text{pre}}/P_{u,\exp}$
A350-0.5-1	84.9	5.71	14.1	0.047	0.293	0.511	153.1	81.2	0.96
A350-0.5-2	86.4	5.91	14.0	0.047	0.311	0.579	161.8	82.6	0.96
A350-1.0-1	108.5	8.49	13.7	0.053	0.439	0.882	197.2	99.0	0.91
A350-1.0-2	109.2	8.87	13.5	0.059	0.476	0.875	199.7	101.2	0.93
A350-2.0-1	126.2	13.73	14.0	0.078	0.691	1.345	240.3	125.9	1.00
A350-2.0-2	123.8	—	—	—	—	—	—	125.9	1.02
Mean	—	—	—	—	—	—	—	—	0.96
Coefficient of variation (COV)	—	—	—	—	—	—	—	—	0.04

Table 3. It can be seen that the parameters δ_1, δ_2, and δ_f increased gradually with increasing adhesive thickness, however, the peak interfacial shear stress seemed to be independent of the adhesive thickness. A similar finding for the interfacial shear stress have been reported with regard to the linear adhesive bonded joints (Xia and Teng 2005; Yu et al. 2012).

By comparing with the existing studies (Xia and Teng 2005; Akbar et al. 2010; Yu et al. 2012; Wu et al. 2012), it can be found that the bond-slip relationship for the CFRP-to-steel bonded joints with a nonlinear adhesive was obviously different from that for the bonded joints with a linear adhesive. The bond-slip relationship for the bonded joints with a linear adhesive was an approximate bilinear shape, which was similar to that for the FRP-to-concrete bonded joints. This pronounced difference was mainly due to the mechanical properties of the adhesive used. For the bonded joints with a nonlinear adhesive, the strong nonlinearity of the adhesive can maintain the shear stress even if the relative slip was large, leading to an approximately stress plateau in the bond-slip relationship. In addition, the bond-slip relationships for the CFRP plate-to-steel bonded joints were only applicable to the case in which the debonding occurred within the adhesive layer (i.e., cohesive failure mode).

The interfacial fracture energy (G_f), which is equal to the area below the bond-slip curve, is an important parameter for the interfacial bond behavior (Wu et al. 2002). The interfacial fracture energy values for the various specimens are listed in Table 3; these values were extracted by averaging the integral values of the experimental bond-slip curves at several points along the bonded interface. Table 3 shows that the interfacial fracture energy increased as the adhesive thickness increased from 0.5 to 2.0 mm. According to the fracture-mechanics-based approach, it can be known that the ultimate load was dependent on the interfacial fracture energy for both the bilinear and trapezoidal bond-slip models (Yuan et al. 2004; Fernando et al. 2014). Therefore, it was the increase of the interfacial fracture energy that resulted in the increase of the ultimate load as the adhesive thickness increased. The ultimate load for such CFRP-to-steel single-shear bonded joints can be determined using Eq. (4) (Taljsten 1994; Chen and Teng 2001; Yuan et al. 2004; Fernando et al. 2014)

$$P_u = b_f\sqrt{2G_fE_ft_f} \tag{4}$$

where b_f = width of the CFRP plate; G_f = interfacial fracture energy; and P_u = ultimate load. The predicted results, $P_{u,\text{pre}}$, are listed in Table 3. It can be seen that the predicted results had a good agreement with the test results. The ratios between the predicted and test results had a mean value of 0.96 and a coefficient of variation (COV) of 0.04. This demonstrated that the fracture-mechanics-based method can be used to predict the ultimate load of CFRP-to-steel bonded joints with desirable accuracy. In addition, the comparative results also implied that the interfacial fracture energy obtained from 3D-DIC measurement had reasonable accuracy.

Effective Bond Length

The preceding test results have showed that the effective bond length existed for such CFRP plate-to-steel bonded joints. For the trapezoidal bond-slip curve, the effective bond length of a bonded interface can be evaluated based on the following equations (Fernando et al. 2014):

$$L_{\text{eff}} = L_d + L_e + \frac{1}{\lambda_1}\ln\frac{1+C}{1-C} \tag{5}$$

where

$$L_d = \frac{1}{\lambda_1}\left[\sqrt{\left(2\frac{\delta_2}{\delta_1}-1\right)}-1\right] \tag{6}$$

$$L_e = \frac{1}{\lambda_2}\arcsin\left[\frac{\lambda_2\lambda}{0.97\delta_1\lambda_1^2}(\delta_f-\delta_2)\right] \tag{7}$$

$$C = \frac{\lambda_2}{\lambda_1\delta_1}(\delta_f-\delta_2)\cot(\lambda_2L_e) - \lambda_1L_d \tag{8}$$

where

$$\lambda^2 = \frac{\tau_{\max}^2}{2G_f}\left(\frac{1}{E_ft_f}+\frac{b_f}{E_st_sb_s}\right) \tag{9}$$

$$\lambda_1^2 = \frac{\tau_{\max}}{\delta_1}\left(\frac{1}{E_ft_f}+\frac{b_f}{E_st_sb_s}\right) \tag{10}$$

$$\lambda_2^2 = \frac{\tau_{\max}}{(\delta_f-\delta_2)}\left(\frac{1}{E_ft_f}+\frac{b_f}{E_st_sb_s}\right) \tag{11}$$

where E_s = elastic modulus of the steel substrate; and t_s and b_s = thickness and width of the steel substrate, respectively. Based on the Eqs. (5)–(11) and the bond-slip parameters (Table 3), the effective bond length for the specimens with different adhesive thicknesses are listed in Table 3. It can be seen that the effective bond length increased with the increase of the adhesive thickness, demonstrating the specimens with thicker adhesive had larger shear stress distribution lengths. The effective bond length increased from 157.5 to 240.3 mm when the adhesive thickness increased from 0.5 to 2.0 mm for such CFRP-to-steel bonded joints.

Conclusions

To further understand the behavior of CFRP plate-to-steel bonded joints with a nonlinear adhesive, a series of single-shear tests were conducted in this paper. The 3D-DIC technique was used

to measure the displacement and strain data. The following conclusions can be drawn based on the presented experimental findings:

- Under the conditions of the parameters studied in this paper, debonding occurred within the adhesive layer for all specimens, indicating a cohesive failure mode;
- Ultimate load gradually increased with increasing bond length until the effective bond length was reached, after which the ultimate load remained approximately unchanged with further increases in the bond length. The ultimate load increased as the adhesive thickness increased from 0.5 to 2.0 mm. The ultimate load for such CFRP-to-steel bonded joints can be predicted by the fracture-mechanics-based method with acceptable accuracy;
- The bond-slip relationship can be simplified to a trapezoidal shape for CFRP plate-to-steel interfaces with the nonlinear adhesive Araldite-2015. The key parameters of δ_1, δ_2, and δ_f increased with an increase in the adhesive thickness; however, the peak shear stress seemed to be independent of the adhesive thickness. The interfacial fracture energy G_f and the effective bond length L_{eff} also increased with the increase of the adhesive thickness. Due to the limited variable ranges addressed in this study, further research is needed to develop a quantitative bond-slip model considering more variables; and
- The 3D-DIC method can collect richer displacement and strain data and is suitable for testing the interfacial behavior between CFRP plates and steel substrates.

Acknowledgments

The authors would like to acknowledge the financial support from the National Basic Research Program of China (No. 2012CB026200), the National Natural Science Foundation of China (No. 51525801), and the Project Funded by the Priority Academic Program Development of Jiangsu Higher Education Institutions (PAPD).

References

Akbar, I., Oehlers, D. J., and Mohamed Ali, M. S. (2010). "Derivation of the bond-slip characteristics for FRP plated steel members." *J. Constr. Steel. Res.*, 66(8–9), 1047–1056.

Ali-Ahmad, M., Subramaniam, K., and Ghosn, M. (2006). "Experimental investigation and fracture analysis of debonding between concrete and FRP sheets." *J. Eng. Mech.*, 10.1061/(ASCE)0733-9399(2006)132:9(914), 914–923.

Al-Mosawe, A., Al-Mahaidi, R., and Zhao, X. L. (2015). "Effect of CFRP properties, on the bond characteristics between steel and CFRP laminate under quasi-static loading." *Constr. Build. Mater.*, 98, 489–501.

Al-Saidy, A. H., Klaiber, F. W., and Wipf, T. J. (2004). "Repair of steel composite beams with carbon fiber-reinforced polymer plates." *J. Compos. Constr.*, 10.1061/(ASCE)1090-0268(2004)8:2(163), 163–172.

Bocciarelli, M., Bocciarelli, P., Fava, G., and Poggi, C. (2009). "Prediction of debonding strength of tensile steel/CFRP joints using fracture mechanics and stress based criteria." *Eng. Fract. Mech.*, 76(2), 299–313.

Carloni, C., Subramaniam, K. V., Savoia, M., and Mazzotti, C. (2012). "Experimental determination of FRP-concrete cohesive interface properties under fatigue loading." *Compos. Struct.*, 94(4), 1288–1296.

Chen, J. F., and Teng, J. G. (2001). "Anchorage strength models for FRP and steel plates bonded to concrete." *J. Struct. Eng.*, 10.1061/(ASCE)0733-9445(2001)127:7(784), 784–791.

Chinese Standard. (2003). "Code for design of steel structures." *GB 50017-2003*, China Planning Press, Beijing (in Chinese).

Dai, J. G., Gao, W. Y., and Teng, J. G. (2013). "Bond-slip model for FRP laminates externally bonded to concrete at elevated temperature." *J. Compos. Constr.*, 10.1061/(ASCE)CC.1943-5614.0000337, 217–228.

Dehghani, E., Daneshjoo, F., Aghakouchak, A. A., and Khaji, N. (2012). "A new bond-slip model for adhesive in CFRP-steel composite systems." *Eng. Struct.*, 34, 447–454.

Deng, J., and Lee, M. M. K. (2007). "Behaviour under static loading of metallic beams reinforced with a bonded CFRP plate." *Compos. Struct.*, 78(2), 232–242.

Fawzia, S., Zhao, X. L., and Al-Mahaidi, R. (2010). "Bond-slip models for double strap joints strengthened by CFRP." *Comp. Struct.*, 92(9), 2137–2145.

Fernando, D., Teng, J. G., Yu, T., and Zhao, X. L. (2013). "Preparation and characterization of steel surfaces for adhesive bonding." *J. Compos. Constr.*, 10.1061/(ASCE)CC.1943-5614.0000387, 04013012.

Fernando, D., Yu, T., and Teng, J. G. (2014). "Behavior of CFRP laminates bonded to a steel substrate using a ductile adhesive." *J. Compos. Constr.*, 10.1061/(ASCE)CC.1943-5614.0000439, 04013040.

Ghiassi, B., Xavier, J., Oliveira, D. V., and Lourenço, P. B. (2013). "Application of digital image correlation in investigating the bond between FRP and masonry." *Compos. Struct.*, 106, 340–349.

Harries, K. A., Peck, A. J., and Abraham, E. J. (2009). "Enhancing stability of structural steel sections using FRP." *Thin Wall Struct.*, 47(10), 1092–1101.

Heshmati, M., Haghani, R., and Al-Emrani, M. (2015). "Environmental durability of adhesively bonded FRP/steel joints in civil engineering applications: State of the art." *Compos., Part B*, 81, 259–275.

Hollaway, L. C., and Cadei, J. (2002). "Progress in the technique of upgrading metallic structures with advanced polymer composites." *Prog. Struct. Eng. Mater.*, 4(2), 131–148.

Kalfat, R., and Al-Mahaidi, R. (2014). "Experimental investigation into the size effect of bidirectional fiber patch anchors in strengthening of concrete structures." *Compos. Struct.*, 112, 134–145.

Kim, Y. J., and Brunell, G. (2011). "Interaction between CFRP-repair and initial damage of wide-flange steel beams subjected to three-point bending." *Compos. Struct.*, 93(8), 1986–1996.

Kim, Y. J., LaBere, J., and Yoshitake, I. (2013). "Hybrid epoxy-silyl modified polymer adhesives for CFRP sheets bonded to a steel substrate." *Compos: Part B*, 51, 233–245.

Liu, H. B., Al-Mahaidi, R., and Zhao, X. L. (2009). "Experimental study of fatigue crack growth behaviour in adhesively reinforced steel structures." *Compos. Struct.*, 90(1), 12–20.

Lu, X. Z., Teng, J. G., Ye, L. P. and Jiang, J. J. (2005). "Bond-slip models for FRP sheets/plates bonded to concrete." *Eng. Struct.*, 27(6), 920–937.

PMLAB 3D-DIC [Computer software]. PMLAB Sensor Tech., Nanjing, China.

Sallam, H. E. M., Badawy, A. A. M., Saba, A. M., and Mikhail, F. A. (2010). "Flexural behavior of strengthened steel-concrete composite beams by various plating methods." *J. Constr. Steel. Res.*, 66(8–9), 1081–1087.

Shi, J. W. (2014). "Durability and reliability design of FRP strengthened concrete structures under coupled effect of multi-factors." Ph.D. thesis, Southeast Univ., Nanjing, China.

Shi, J. W., Zhu, H., Wu, Z. S., Seracino, R., and Wu, G. (2013). "Bond behavior between basalt fiber-reinforced polymer sheet and concrete substrate under the coupled effects of freeze-thaw cycling and sustained load." *J. Compos. Constr.*, 10.1061/(ASCE)CC.1943-5614.0000349, 530–542.

Taljsten, B. (1994). "Plate bonding: Strengthening of existing concrete structures with epoxy bonded plates of steel or fibre reinforced plastics." Ph.D. thesis, Lulea, Univ. of Technology, Lulea, Sweden.

Teng, J. G., Yu, T., and Fernando, D. (2012). "Strengthening of steel structures with fiber-reinforced polymer composites." *J. Constr. Steel. Res.*, 78, 131–143.

Wang, H. T., and Wu, G. (2015). "Experimental study on the fatigue behavior of CFRP-to-steel bonded interface." *12th Int. Symp. on Fiber Reinforced Polymers for Reinforced Concrete Structures & the 5th Asia-Pacific Conf. on Fiber Reinforced Polymers in Structures Joint Conf.*, International Institute for FRP in Construction, Nanjing, China.

Wang, H. T., Wu, G., and Jiang, J. B. (2015). "Fatigue behavior of cracked steel plates strengthened with different CFRP systems and configurations." *J. Compos. Constr.*, 10.1061/(ASCE)CC.1943-5614.0000647, 04015078.

Wu, C., Zhao, X. L., Duan, W. H., Al-Mahaidi, R. (2012). "Bond characteristics between ultra high modulus CFRP laminates and steel." *Thin. Wall. Struct.*, 51, 147–157.

Wu, Y. F., and Jiang, C. (2013). "Quantification of bond-slip relationship for externally bonded FRP-to-concrete joints." *J. Compos. Constr.*, 10.1061/(ASCE)CC.1943-5614.0000375, 673–686.

Wu, Z. S., Yuan, H. and Niu, H. D. (2002). "Stress transfer and fracture propagation in different kinds of adhesive joints." *J. Eng. Mech.*, 10.1061/(ASCE)0733-9399(2002)128:5(562), 562–573.

Xia, S. H., and Teng, J. G. (2005). "Behavior of FRP-to-steel bond joints." *Proc., Int. Symp. on Bond Behaviour of FRP in Structures*, International Institute for FRP in Construction, Hong Kong.

Yu, T., Fernando, D., Teng, J. G., and Zhao, X. L. (2012). "Experimental study on CFRP-to-steel bonded interfaces." *Compos., Part B*, 43(5), 2279–2289.

Yuan, H., Teng, J. G., Seracino, R., Wu, Z. S., and Yao, J. (2004). "Full-range behavior of FRP-to-concrete bonded joints." *Eng. Struct.*, 26(5), 553–565.

Zhao, X. L., Bai, Y., Al-Mahaidi, R., and Rizkalla, S. (2013). "Effect of dynamic loading and environmental conditions on the bond between CFRP and steel: State-of-the-art review." *J. Compos. Constr.*, 10.1061/(ASCE)CC.1943-5614.0000419, A4013005.

Zhao, X. L., and Zhang, L. (2007). "State-of-the-art review on FRP strengthened steel structures." *Eng. Struct.*, 29(8), 1808–1823.